JMEPEG
https://doi.org/10.1007/s11665-023-08727-2

1059-9495/$19.00

ORIGINAL RESEARCH ARTICLE

The Role of Calcination Temperature in the Self-cleaning Functionality of Urea-Doped TiO_2 Prepared through In Situ Heat-Assisted Sol–Gel Synthesis

Valantine Takwa Lukong, Christopher Nonso Chukwuati, Kingsley Ukoba, and Tien-Chien Jen

Submitted: 11 December 2022 / Revised: 29 August 2023 / Accepted: 8 September 2023

In this study, urea-doped titanium dioxide (urea-TiO_2) nanoparticles were synthesized through an in situ heat-assisted sol–gel technique using titanium (IV) isopropoxide as the precursor for titanium dioxide and urea as a nitrogen source. The nanoparticles were calcined at 300, 500, and 700 °C to study the effect of the calcination temperature on their function as self-cleaning material. The nanoparticles were characterized using a scanning electron microscope and a transmission electron microscope for morphology, X-ray diffraction, Raman spectroscopy, and Fourier transformed infrared spectroscopy for structure, UV–Vis, and photoluminescence spectroscopy for optical analysis. The self-cleaning study was carried out by letting samples degrade methylene blue and Rhodamine-B under UV irradiation. The morphological analysis reveals particle size distribution with more disparity at higher calcination temperatures. At lower calcination temperatures, the dopant caused high clustering of particles, keeping them linked together in muddy form and layers. Structural analysis showed that the particles were nanostructured with average crystallite sizes ranging from 2.35 to 16.13 nm and phase transformation from anatase to rutile after calcining at 700 °C. The nitrogen presence created a lattice disorder in the TiO_2 structure, and the impact of higher calcination temperature on the nanoparticles further shifted the band toward a higher wavenumber under FTIR analysis. The optical bandgap reduced from 3.29 eV at 300 °C to 3.09 eV at 700 °C. The determined values of the rate constant from the photodegradation test showed that the highest rate was obtained at 700 °C, indicating enhanced self-cleaning functionality with an increase in calcination temperature of urea-TiO_2.

Keywords characterization: rhodamine-B, photocatalysis, self-cleaning, temperature variation

1. Introduction

Materials with self-cleaning qualities continue to be in high demand in many applications such as photovoltaic surfaces (Ref 1), car bodies (Ref 2), window glass (Ref 3), water purification (Ref 4), building surfaces (Ref 5), medical equipment (Ref 6), and tarred road surfaces (Ref 7). Any substance that can degrade, disseminate, and rebuff contaminants or dirt off its surface without external assistance is a self-cleaning material. These materials are inculcated into surfaces to be either hydrophilic or hydrophobic. In the former, water molecules in contact with the surface roll and pick up dirt away from the surface. In the latter, the water molecules spread over the surface, chemically breaking down and absorbing dirt off the application surface. Materials suitable for self-cleaning must be long-lasting, cheap, non-poisonous, anti-corrosive, and stable chemically and mechanically (Ref 8). One common material possessing most of these qualities is titanium dioxide (TiO_2) (Ref 9). It is a superset photocatalyst known to degrade several environmental pollutants due to its robust oxidizing ability, resistance to heat, and chemical sturdiness (Ref 10). TiO_2 is found naturally in three different crystal forms (anatase, rutile, and brookite) with optical bandgaps of 3.0, 3.21, and 3.13 eV, respectively, (Ref 11). This wide bandgap of TiO_2 restricts the amount of solar energy it can absorb, thereby limiting its photocatalytic and, thus, self-cleaning ability under sunlight (Ref 12, 13).

Numerous methods have been investigated to enhance the photoresponse and self-cleaning functionality of TiO_2 nanocomposites to address this rudimentary problem. Ilkhechi et al. conducted an extensive study on TiO_2 to address this limitation and enhance its optical properties by doping it with other metallic and nonmetallic elements (Ref 14-16). They observed a significant drop in its absorption band edge. Doping is a well-adopted scientific strategy for improving materials' optical, structural, and wettability properties (Ref 17-19). Other methods adopted to improve the photocatalytic properties of TiO_2 include: exciting it with other low band gap materials such as CdS and PbS (Ref 20, 21), fine-tuning the phase and the crystallite size (Ref 22-25), and synthesis temperature variation and post-synthesis heat treatment (Ref 26-28). Ilkhechi and Kaleji, using the sol–gel method and varying calcination temperatures from 500 to 1000 °C, examined the effects of Zr and Si dopants of different concentrations on crystallite size, phase transformation, and photocatalytic activity of titania nanopowders and observed that the doped samples revealed a more vigorous photocatalytic activity than the bare TiO_2 (Ref

Valantine Takwa Lukong, Christopher Nonso Chukwuati, Kingsley Ukoba, and **Tien-Chien Jen**, University of Johannesburg, Auckland Park Campus, Johannesburg 2006, South Africa. Contact e-mail: tjen@uj.ac.za.

Published online: 02 October 2023

29, 30). This enhancement was attributed to the decrease in the rate of photo-generated electron–hole recombination that occurs when Zr4 + and Si4 + substitute Ti4 + in the titania network (Ref 30-32). This enhancement of TiO_2 has increased opportunities for its application and opened doors for further studies.

The doping of TiO_2 with nitrogen has been observed to create a tremendous shift in the absorption band edge of TiO_2 (Ref 33). Above the TiO_2 valence band, the nitrogen 2p states give rise to permitted energy levels. The visible-light activity of these doped systems is explained by the metal, which provides permissible energy gaps not far from the conduction ring and the transition from the proper 2p nitrogen positions to the conduction band (Ref 34, 35). Urea is a hydrocarbon with a high nitrogen concentration that could be used as a TiO_2 doping agent (Ref 36). Urea-doped TiO_2 nanoparticles have been investigated for different photocatalytic abilities by letting them degrade various types of dyes (Ref 37), altering their synthesis process (Ref 38), and varying their doping concentration on the different synthesis routes (Ref 39, 40).

The outcomes of the investigations in the preceding paragraph all confirmed that urea-doped TiO_2 is very photocatalytic and, thus, suitable for self-cleaning applications. The sol–gel method has also been a popular choice for its synthesis owing to its ease of control, simplicity, and capability of mass production at a low cost. But, the clustering of particles from this method requires a post-synthesis heat treatment for better crystal anatomy and uniform distribution of the particles. However, the influence of post-synthesis heat treatment on urea-TiO_2 has yet to be adequately reported in the open literature. In this paper, an in situ sol–gel method assisted by heat was adopted to synthesize urea-TiO_2 nanoparticles, and the effect of the calcination temperature on the urea-TiO_2 nanoparticles was investigated. The doping helped to sensitize the light visibility of TiO_2 powders with interstitial molecular architectures of nitrogen and its self-cleaning ability under different temperatures were examined.

2. The Experiment

2.1 Materials

The materials used in this experiment and their suppliers are indicated in Table 1.

2.2 In Situ Synthesis of Urea-doped TiO_2

The synthesis of the urea-doped TiO_2 was done in situ. The chemicals used were all obtained in analytical grades and administered as such. First, 97% titanium (IV) isopropoxide was solvated in 99.9% ethanol at a ratio of 1:5 while stirring. After 30 minutes, the solution was gradually added with acid stock—made by mixing nitric acid and de-ionized water in a 1:50 ratio—while under 500 rpm magnetic agitation. After 30 more minutes of agitation, 5wt% urea solution was put in the mix dropwise. The entire combination was then swirled again for 1 hour and 30 minutes while being heated at 60 °C to ensure proper hydrolysis. Afterward, the TiO_2 nanoparticles were dried in an oven for 24 hours at 100 °C. For temperature fine-tuning, the resulting urea-TiO_2 nanoparticles were heat treated at 300, 500, and 700 °C for one hour.

2.3 Characterization

With an x-ray diffractometer (PHILIP-XPERT PRO), Raman spectroscopy (class 1 Laser thermos-scientific DXR2 SmartRaman), and Fourier transformed infrared spectroscopy (SHIMADZU 2450), the produced urea-doped TiO_2 nanoparticles were examined for structural properties. A TESCAN (Oxford Instruments, VEGA3 X-MAX) SEM and a JEOL JEM 2100 80 T X-MAX TEM were used for morphological studies. ImageJ was further employed to examine the grain size and distribution. The optical characteristics were investigated by employing a UV-2450 spectrophotometer and an RF-6000 spectrofluorophotometer (Shimadzu) at an excitation wavelength of 220 nm and a scan speed of 6000 nm/min. An MB and RhB dye degradation tests were performed under UV irradiation using 40 W, 40-cm-long T5 BLB lamps for self-cleaning analysis. The test tube was 5 cm below the UV lamp and 10 cm deep throughout the experiment. With the help of DF-L 0.22-μm filters, the urea-TiO_2 catalyst was separated after UV irradiation. The concentrations of the dyes in the samples taken at 30-minute intervals were studied with a UV-2450 spectrophotometer (Shimadzu).

3. Results and Discussion

3.1 Morphological Analysis

Detailed morphological analysis and the grain size distribution of the urea-doped TiO_2 samples are shown in Figure 1. Figure 1(a), (b), and (c) depicts SEM images obtained after calcination at 300, 500, and 700 °C, respectively. It is observed that the urea dopant impacted the high clustering of the particles at low temperatures keeping the particles glued together in muddy form with spaces between the layers, similar to Ananpattarachai et al. (Ref 41). But as the calcination temperature is raised from 300 to 700 °C, the particles are seen to be increasingly powder-like with different shapes and sizes.

Table 1 List of chemicals, their suppliers, and their functions

Materials	Chemical formula	Supplier	Function
Urea powder	NH_2CONH_2	Sigma-Aldrich, USA	Dopant and nitrogen source
97% Titanium(IV) isopropoxide	$Ti[OCH(CH_3)_2]_4$	Sigma-Aldrich, Germany	Precursor for TiO_2 synthesis
99% Ethanol	CH_3CH_2OH	Merck Chemicals, SA	Synthesis solvent
70% Nitric acid	HNO_3	Sigma-Aldrich, Germany	As stabilizer
De-ionized water	H_2O	Merck Chemicals, SA	To hydrolyze the solution

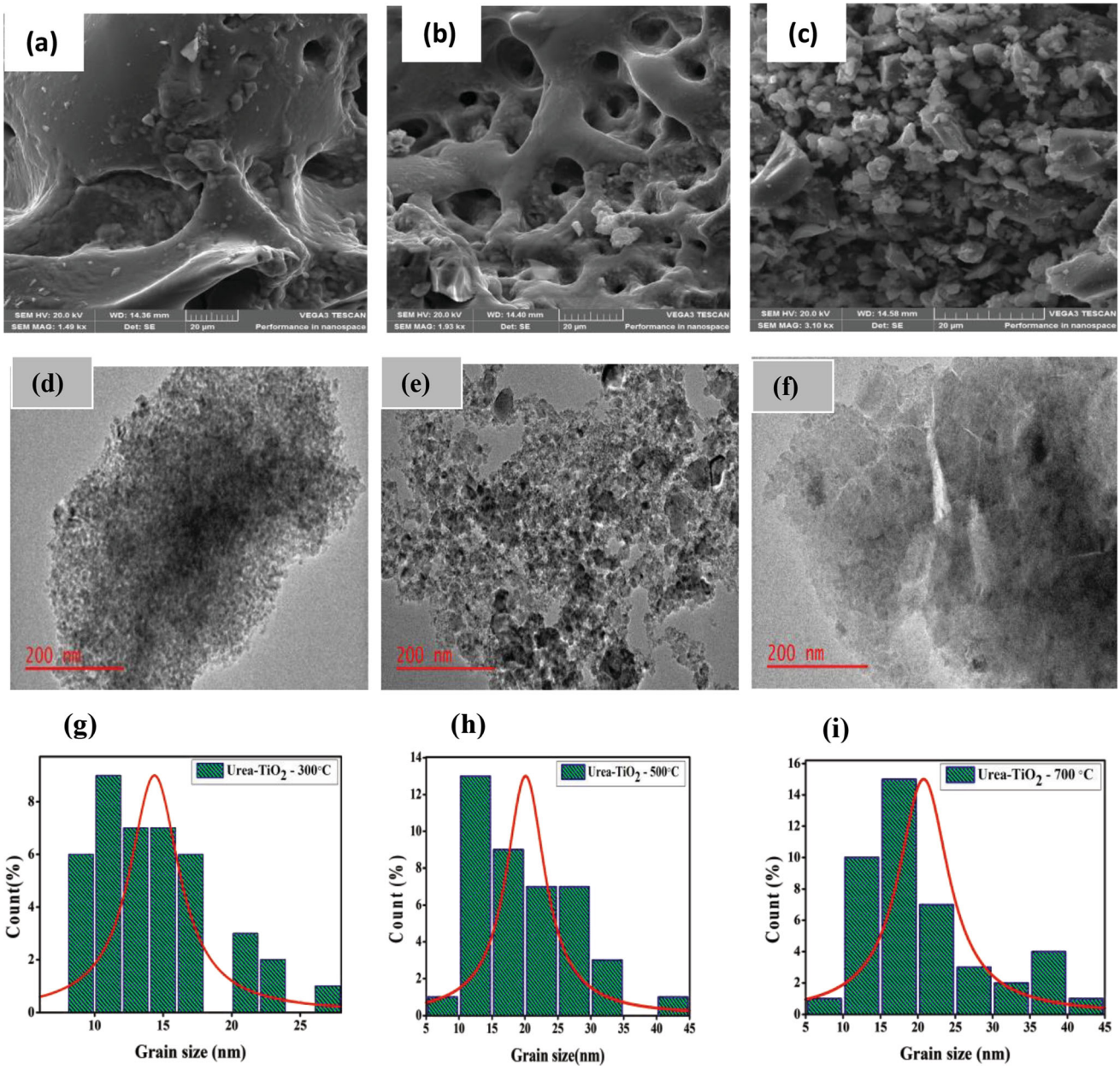

Fig. 1 (a), (b), and (c) are SEM micrographs of urea-TiO_2 calcined at 300, 500, and 700 °C, respectively. (d), (e), and (f) are TEM images for samples calcined at 300, 500, and 700 °C, respectively, and (g), (h), and (i), respectively, depict grain size and Gaussian distribution at 300, 500, and 700 °C

The TEM analysis obtained at 200 nm magnification is shown in Figure 1(d), (e), and (f) for specimens calcined at 300, 500, and 700 °C, respectively.

All the specimens showed tiny particle agglomeration, especially at 300 °C. As the calcination temperature was raised, the agglomerated particles were observed to have formed layers. The average particle size with their Gaussian distribution graph for the TEM images analyzed using ImageJ is shown in Figure 1(g), (h), and (i) for the respective calcination temperatures. The average particle size increased as the temperatures were raised, with the size of 2.42, 10.42, and 16.96 nm obtained at 300, 500, and 700 °C, respectively.

The grain size distribution plot revealed a more significant disparity in particle size at 700 °C than at 300 and 500 °C. This may result from the high transformation from the anatase to the rutile phase. Uniform particle distribution is desired for better photocatalytic and self-cleaning applications of urea-doped TiO_2 (Ref 42).

3.2 Structural Analysis

XRD and Raman's spectroscopy were used to analyze the structural composition of the created urea-TiO_2 nanoparticles. The XRD patterns of urea-TiO_2 samples at varied annealing temperatures are displayed in Figure 2. The peak intensities increased with an increase in calcination temperature. The appropriate miler indices are given in brackets, and the XRD peaks are identified as (A) for the anatase and (B) for the rutile phase. Both anatase and rutile phases were displayed in all the samples. At 300 °C, the XRD peaks mainly were anatase, with

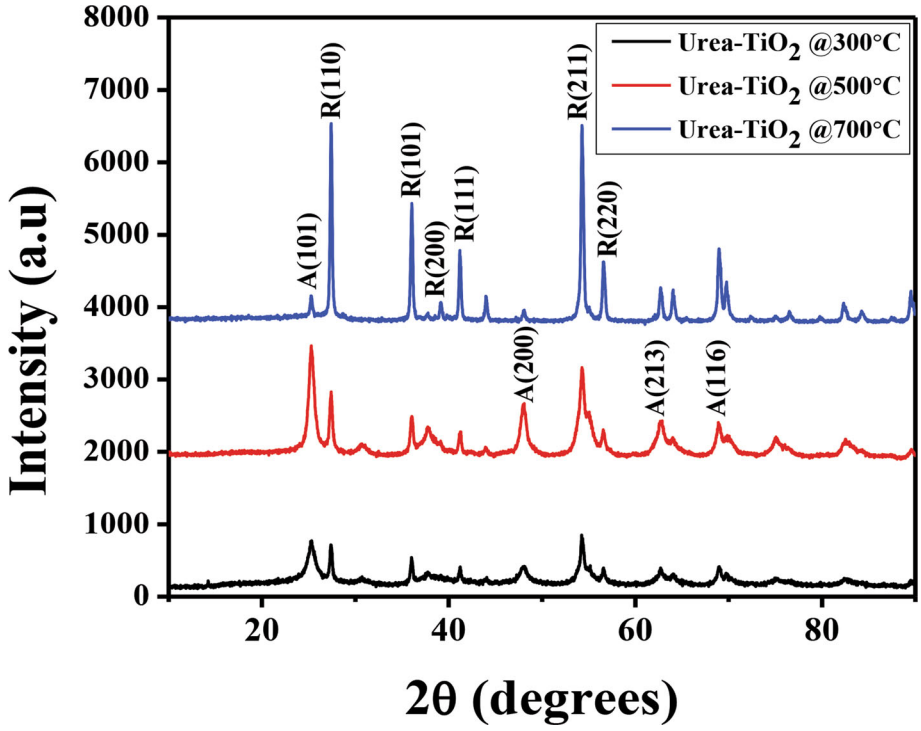

Fig. 2 The diffraction patterns of urea-TiO_2 calcined at 300, 500, and 700 °C

major ones appearing at 2θ equal to 25.49, 47.95, 62.77, and 68.99. These angles matched the *hkl* planes of (101), (200), (213), and (116), respectively (ICDD card (04-011-0664), while the few rutile visible peaks appeared at 2θ values of 27.39, 35.99, and 54.33 (ICDD card 04-003-0648) corresponding to *hkl* planes of (110), (101), and (111) As the temperature was raised to 500 °C, the anatase peaks were seen to be very prominent, a sign of better crystallinity. Few rutile peaks appeared, showing that phase transformation is already taking place. At the calcination temperature of 700 °C, more rutile peaks became prominent, indicating that most anatase urea-TiO_2 nanoparticles have transformed into the rutile phase. The most significant rutile peak was found in the patterns for 700 °C at 27.39°, which corresponds to the *hkl* plane of *R* (1 1 0), and the most significant anatase peak occurred at 2θ equals 25.30 and is for the pattern calcined at 500 °C. The lower concentration of the urea species used as a nitrogen source resulted in most of the dopants being absorbed into the interstitial spaces of TiO_2, leaving no visible nitrogen peak in the XRD patterns (Ref 43).

The average crystallite size (D) was evaluated using the Debye–Scherrer formula, as shown in Equation 1 (Ref 44).

$$D = {}^{k\lambda}/_{\beta \cos\theta} \quad \text{(Eq 1)}$$

where D is in (nm^2), β in radians denotes the full width at half maximum (FWHM), the wavelength (nm) is represented by λ, the Bragg's diffraction angle θ, and k is the shape constant taken (0.94). The dislocation density, δ, and the spacing between parallel atomic planes, d, were evaluated using Equations (2) and (3), respectively, while the values of the lattice constants were calculated using Equation (4) (Ref 45), with Miller indices of $A(200)$ used as legends for the anatase phase and $R(002)$ for the rutile phase

$$\delta = {}^{1}/_{D^2} \quad \text{(Eq 2)}$$

$$d = \frac{\lambda}{2\sin\theta} \quad \text{(Eq 3)}$$

$$\frac{1}{d^2} = \frac{h^2 + k^2}{a^2} + \frac{l^2}{c^2} \quad \text{(Eq 4)}$$

The range of average crystallite sizes was 2.35-16.13 nm, considering all the phases as recorded in Table 2 together with the values computed for the lattice constants (a and c) of the urea-doped TiO_2 nanoparticles for the various calcination temperatures. The nanoparticles' microstrain values were calculated using Equation (5).

$$\varepsilon = {}^{\beta}/_{4\tan\theta} \quad \text{(Eq 5)}$$

The values of the crystallite sizes were consistent with those obtained by analyzing the TEM images using ImageJ. The increase in crystallite size is associated with the transformation from the anatase to the rutile phases and the agglomeration of smaller particles (Ref 46, 47). The cell volume was calculated using the lattice constants a and c values.

Further examination of the samples' structural features was carried out with Raman spectroscopy, and Figure 3 shows the spectral bands of each. For samples heat treated at 300 °C, six anatase phase transitions were identified at the Raman spectral bands of 145 cm^{-1} (Eg), 197 cm^{-1} (Eg), 397 cm^{-1} (B1g), 518 cm^{-1} (B1g), 640 cm^{-1} (Eg), and 1047 cm^{-1} (A1g) showing a slight shift toward higher wavenumber (Ref 48). At 700 °C calcination temperature, rutile phases are observed with significant peaks at spectral bands of 195, 325, 319, 457, and 607 cm^{-1}, matching spectral indices of (B1g), Eg, (A1g), and (B2g), respectively. The intensities of the peaks increase with

Table 2 Crystal parameters and characteristics of urea-TiO_2 obtained at different calcination temperatures

Cal. temp.	Structure/phase	Space group	2θ°	*hkl*	λ(Å)	FWHM (°)	β (Rads)	D, nm^{-2}	δ, nm^{-2}	d(Å)	ε × 10^{-3}	a(Å)	c(Å)	Cell volume × 10^6(Å3)
300	Tetragonal/anatase	I41/amd	25.29	101	1.5406	0.6172	0.0108	2.35	0.1811	3.5188	34.1792	3.6333	14.0752	185.80	136.93
	Tetragonal/rutile	P42/mnm	27.39	110	1.5406	0.2436	0.0043	14.02	0.0051	3.2536	0.5032	4.6014	6.507	137.77	62.84
500	Tetragonal/anatase	I41/amd	25.29	101	1.5406	0.5073	0.0089	2.86	0.1223	3.5188	28.0932	3.6333	14.0752	185.80	136.36
	Tetragonal/rutile	P42/mnm	27.39	110	1.5406	0.3129	0.0055	10.82	0.0085	3.2536	0.6464	4.6012	6.5072	137.76	62.43
700	Tetragonal/anatase	I41/amd	25.28	101	1.5406	0.2476	0.0043	5.86	0.0291	3.5202	14.6464	3.6356	14.0807	186.11	136.96
	Tetragonal/rutile	P42/mnm	27.39	110	1.5406	0.2121	0.0037	16.13	0.0038	3.2536	0.4381	4.6012	6.5072	137.76	62.74

temperature, confirming better crystallinity as observed with XRD peaks.

The enlarged inset shows a complete upset of peaks at 500 °C calcination temperature with a broader localized peak around the spectral band 231 cm^{-1}, which can be attributed to the transition from anatase to rutile phase. Also, in the inset, band shift toward higher wavenumbers is significant at a calcination temperature of 700 °C, confirming defects introduced by nitrogen in TiO_2 lattice structure at this higher temperature due to changes in particle sizes as seen from XRD results or by oxygen vacancies generated from the interaction of nitrogen and TiO_2 (Ref 49, 50). A comparison of the Raman peaks agrees with the XRD result of increased peak intensities and, thus, crystallinity as the calcination temperature is raised (Ref 51).

Figure 4 shows the patterns of FTIR spectra of the urea-TiO_2 samples for the different calcination temperatures revealing several functional groups on the surface of each nanoparticle. The FTIR molecular fingerprint identifies the vibration pattern of the hydroxyl group (∼OH), an intense ∼ N–O stretching, and the ∼ O–H bending mode at approximately 3424, 1638, and 1379 cm^{-1}, respectively, on the pretreated nanoparticles around 1638 cm^{-1}. The strong N–O stretching band (1638 cm^{-1}) was formed due to nitrogen, indicating the presence of ∼ NH_2 groups on the urea/TiO_2 NPs (Ref 52). The vibrations created by the Ti–N bond are responsible for a small band that appears around 1121 cm^{-1} (Ref 53). O–Ti–O vibrations patterns in TiO_2 are typically found in a broad band between 777 and 468 cm^{-1}(Ref 54). At higher calcination temperatures (700 °C), the ∼ OH vibration band shifted to approximately 3438 cm^{-1}, and the band around 2068 cm^{-1} became less pronounced. The band shift was induced by the presence of ∼ NH_2 (Ref 55), and the impact of higher temperature on the nanoparticles was exposed. A change to a higher wavenumber is usually observed at higher calcination temperatures. The formation of hydroxyl radicals during photocatalytic processes may benefit from the high intensity of bands linked to the O–H group for both the stretching and vibration modes, leading to excellent self-cleaning ability (Ref 56). Besides the above observations, the FTIR patterns did not reveal a significant difference in temperature impact.

3.3 Optical Analysis

The optical properties of urea-doped TiO_2 samples were examined under DRS and photoluminescence spectroscopy. Figure 5(a) displays the absorbance threshold for the urea-doped TiO_2 samples calcined at 300, 500, and 700 °C, and Figure 5(b) displays the samples' plot of $(\alpha h\nu)^2$ against hν. All the samples absorbed light with wavelengths from 750 to 395 nm, showing that absorption capability extended into the visible-light region. This could be possible due to the nitrogen content of the urea dopant (Ref 57). The optical bandgap was estimated from the plot of $(\alpha h\nu)^2$ against hν shown in Figure 5(b) using the relation by Tauc as shown in Equation (6) (Ref 58)

$$(\alpha h\nu)^2 = K(h\nu - Eg) \quad \text{(Eq 6)}$$

Eg stands for the optical energy gap, hν for the incident energy of photons, with α resenting Beer–Lambert's absorption coefficient, and *K* for a constant independent of the energy level.

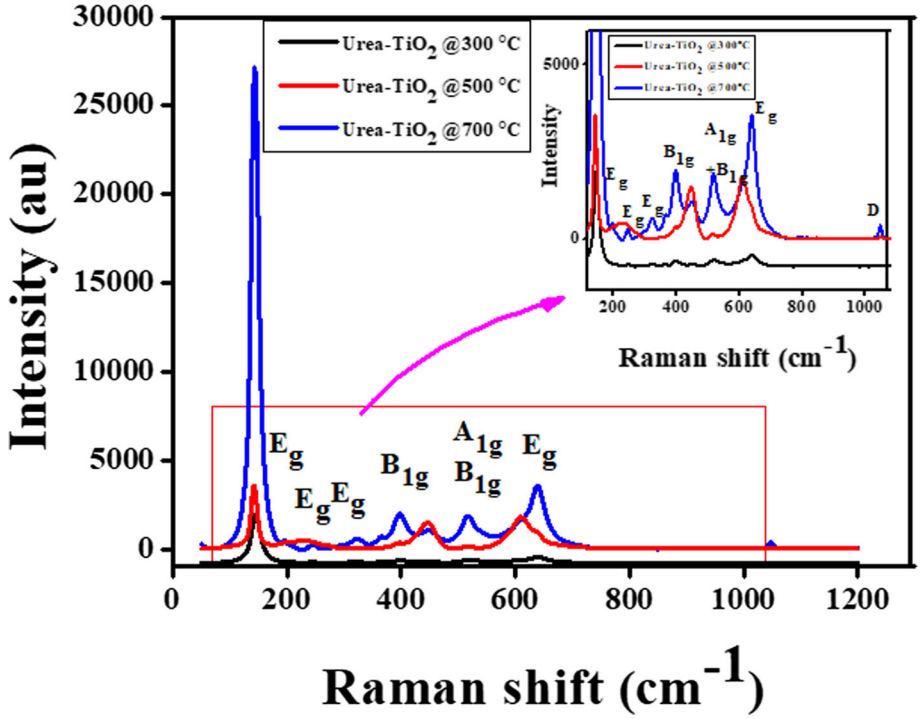

Fig. 3 Raman analysis of urea-TiO_2 calcined at 300, 500, and 700 °C

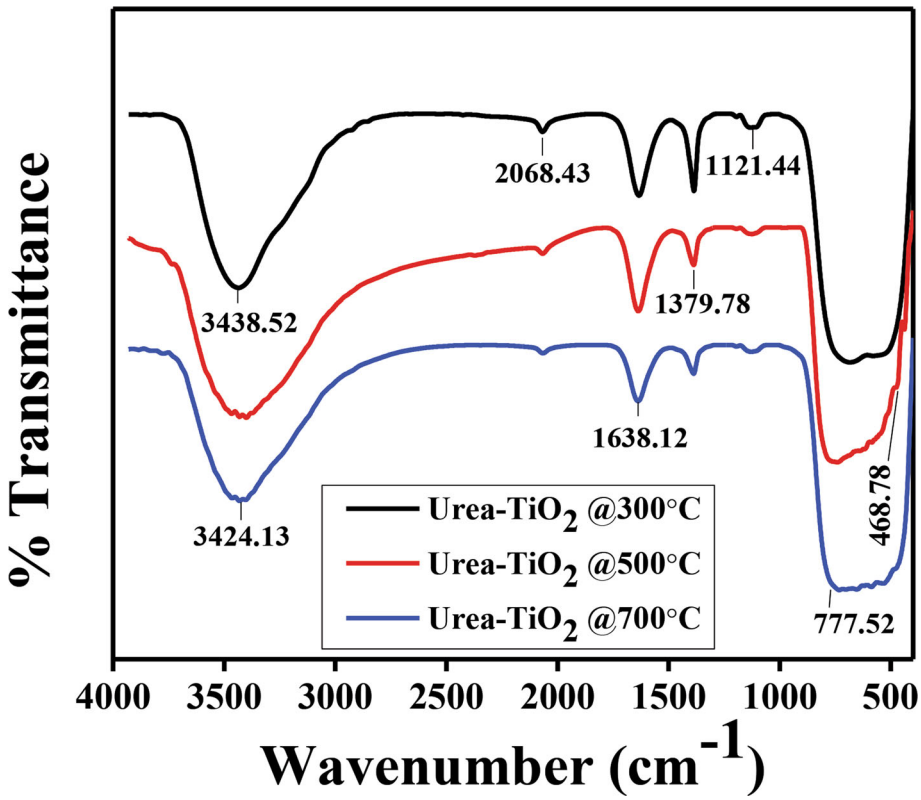

Fig. 4 FTIR spectra of urea-TiO_2 calcined at 300, 500, and 700 °C

The plot revealed a reduction in optical energy gaps with increased calcination temperature. The optical bandgap dropped from 3.29 at 300 °C to 3.09 at 700 °C. Self-cleaning applications benefit from the lower band gap because the nanoparticles will rapidly get functionalized once under visible light. This is attributed to the less energy required to transit from the valence circle to the conduction ring. As shown in Figure 5(a), between 800 and 400 nm, high calcination

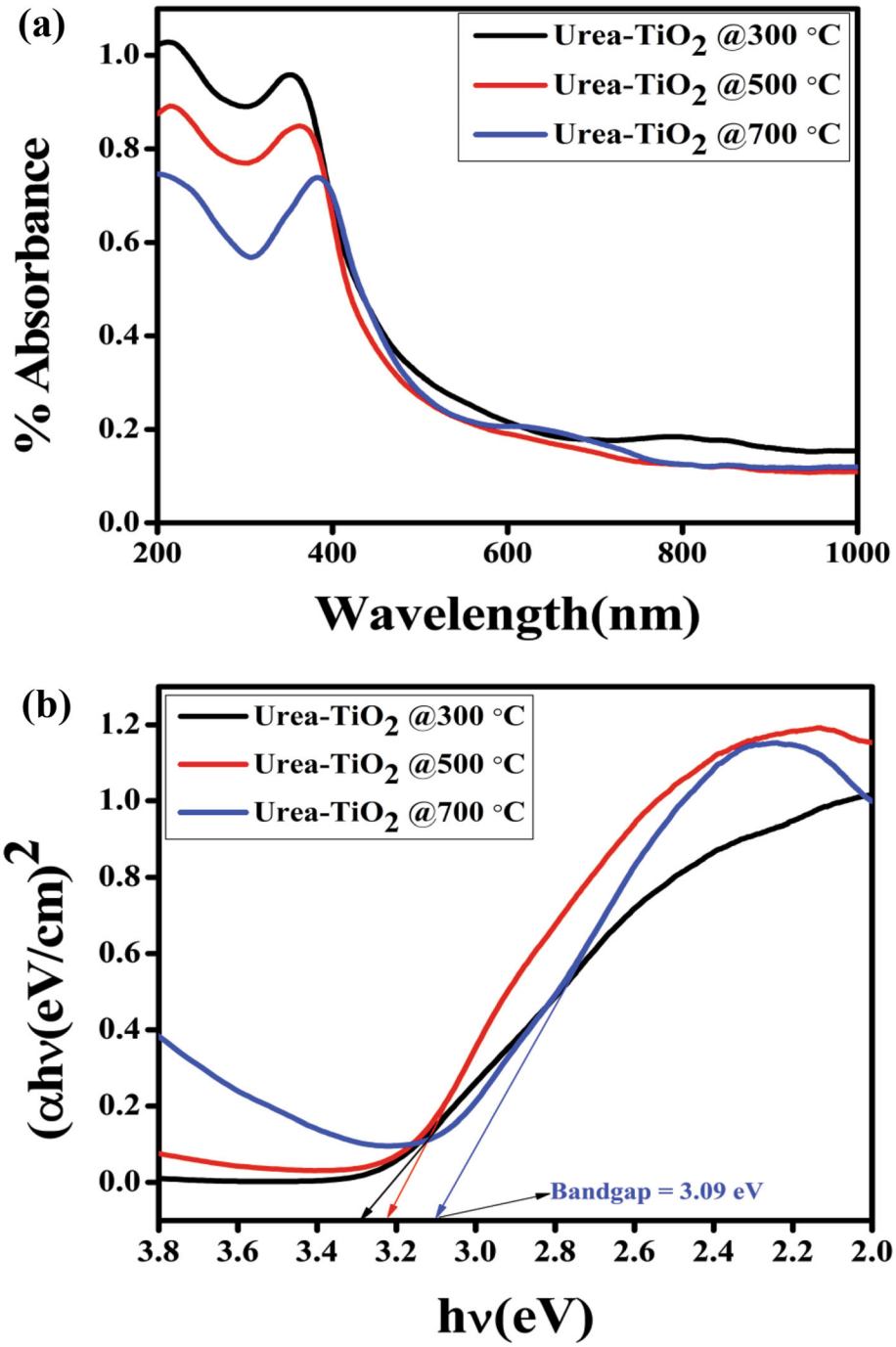

Fig. 5 Optical properties of urea-doped TiO_2: (a) DRS absorbance spectra and (b) graph of $(\alpha h\nu)^2$ against incident energy ($h\nu$), for samples calcined at 300, 500, and 700 °C

temperatures helped remove most of the natural material from the surface of urea-TiO_2 nanoparticles, enhancing its absorption capabilities.

Figure 6 shows the spectra bands of samples for the three different calcination temperatures obtained from Photoluminescence (PL) analyses. The spectra band for the model calcined at 500 and 700 °C shows a shift to higher wavelengths.

The photoluminescence peaks for the sample calcined at 500 °C reflect high crystallinity, which also agrees with the results of the XRD analysis. This can be attributed to the fact that most organic remnants have been eliminated while the N-dopant is still kept, and the anatase TiO_2 is better crystalline at 500 °C than at 300 °C. The better crystallinity of the more anatase content, in the instance of urea-TiO_2, calcined at 500 °C, is responsible for the increase in PL peak intensity. The sample calcined at 700 °C showed a decline in PL peak intensity, possibly due to a decrease in the crystalline anatase content as more transformation to the rutile phase occurs (Ref 59). However, due to the reduced bandgap and the presence of crystalline anatase phases, photoactivity for samples calcined at 700 °C remained high, as affirmed by the photodegradation

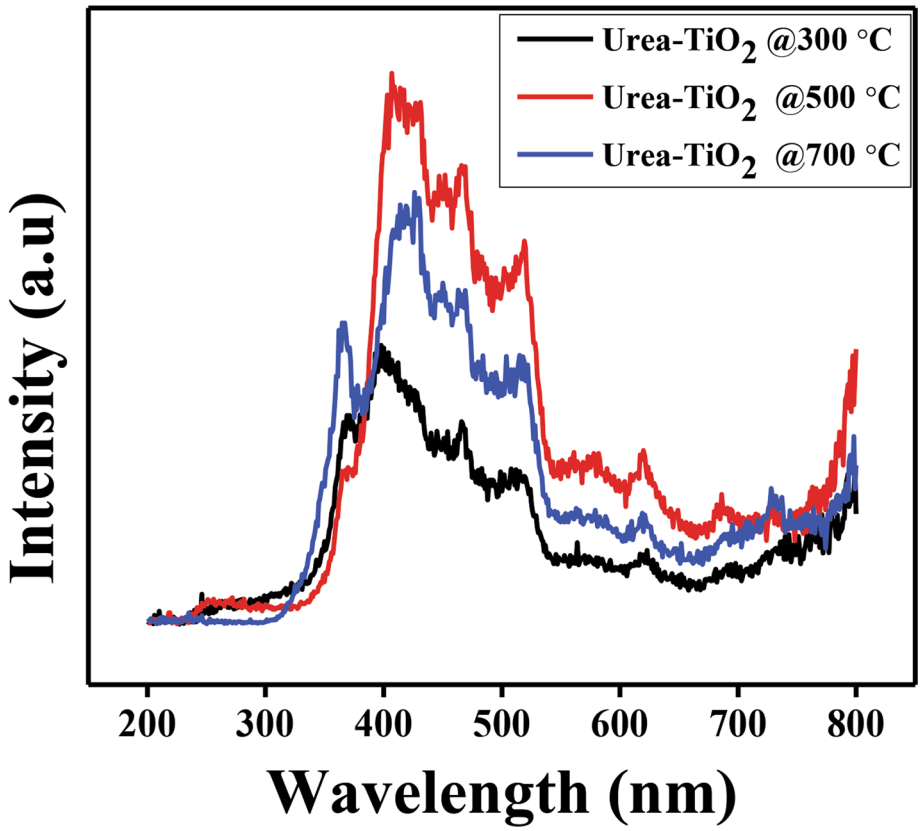

Fig. 6 Photoluminescence spectra of urea-doped TiO_2 calcined at 300, 500, and 700 °C

test. In addition, they extended the absorption ability into the visible-light region due to the presence of nitrogen. At a higher temperature of 700 °C, most organic residues are removed, improving absorption and photocatalytic activity, thereby boasting self-cleaning functionality (Ref 60). At the calcination temperature of 300 °C, most organic residues on the specimen surface were not yet removed, impacting the photocatalytic or self-cleaning activity of the sample (Ref 45).

3.4 Self-cleaning Study

3.4.1 Methylene Blue (MB) Degradation. Fifty milligrams of each sample were liquefied in a 100 ml volume of 10 ppm MB for a photodegradation test under UV irradiation. The degradation efficiency was examined to observe and compare self-cleaning activity based on the calcination temperature. The urea-TiO_2 serves as a photocatalyst in the light-activated process of photocatalytic degradation. When the nanoparticles are exposed to UV radiation, electrons are produced and undergo a chemical reaction that changes water molecules into hydroxyl radicals. These hydroxyl radicals break down the carbon-based filth into smaller pieces that can be easily removed. Figure 7(a), (b) and (c) shows the reduction in MB concentration over time for samples that were heat treated at 300, 500, and 700 °C, respectively. Around the wavelength of 655 nm, all concentrations were seen to exhibit maximum peaks. Under UV exposure from 0 to 120 minutes, all urea-TiO_2 samples efficiently degraded the methylene blue dye. The nanoparticles calcined at 500 and 700 °C exhibited faster degradation activity than at 300 °C, with the most rapid observed sample calcined at 700 °C. Figure 7(d) compares the percentage of MB depletion caused by various urea-TiO_2 samples. The model calcined at 700 °C demonstrated the maximum degradation efficiency of 83.33% during the 120-minute interval of UV exposure, while the pieces calcined at 500 and 300 °C removed 68.52 and 46.29%, respectively, as shown in Table 3.

The graph of $\ln(C_t/C_0)$ against time and the first-order kinetics rate constants evaluated using the Langmuir–Hinshelwood expression shown in Equation (7) for the three samples is shown in Figure 7(e).

$$\ln(C_t/C_0)^{(1/4)} - \mathrm{Kt} \qquad \text{(Eq 7)}$$

C_t denotes the MB content at any time t, C_0 denotes the initial MB content under UV light, and K means the rate constant. The determined values of k, as recorded in Table 3, indicate that higher calcination temperatures resulted in faster photodegradation rates. This results from the fact that the phase transformation from anatase to rutile at higher calcination temperatures increased electron–hole separation and suppressed the charge carrier recombination. With rising temperatures, fewer deep trap states are serving as recombination centers. This decrease in recombination results in a rise in photocatalytic activity due to increased charge carrier lifetime (Ref 61). Also, through the process of calcination, most of the natural material on the surfaces of the urea-TiO_2 nanoparticles was removed, improving their light absorption. Furthermore, improved crystal structure provided more significant surface areas enabling more excellent absorption per particle, enhancing photocatalysis, and making them suitable for self-cleaning. In contrast, at lower calcination temperatures, including nitrogen causes the creation of electron holes, which accelerates

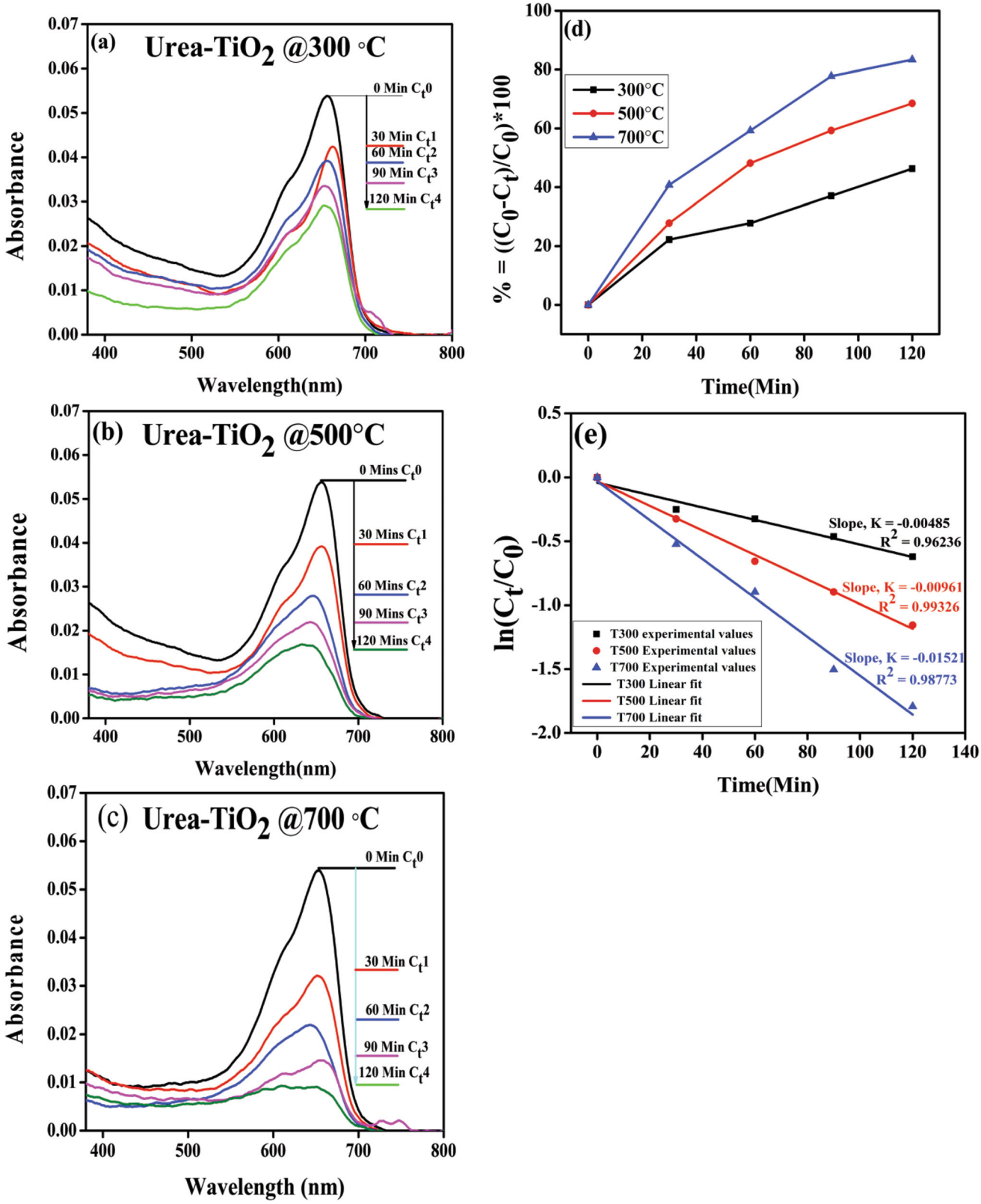

Fig. 7 Self-cleaning analysis; loss of MB content under UV light for (a) 300 °C, (b) 500 °C, and (c) 700 °C, (d) percentage degradation against time for samples annealed at 300 °C, 500 °C, and 700 °C, (e) $\ln(C_t/C_0)$ against the time of degradation for the different calcined samples

Table 3 Summary of calcination temperature effect on the self-cleaning property of urea-TiO_2

Cal. temp	C_0–C_{120}	Percentage degradation	Rate constant k, min^{-1}	Adj. R^2
T300	0.4630	46.30 %	−0.00485	0.96236
T500	0.6852	68.52 %	−0.00961	0.99326
T700	0.8333	83.33 %	−0.01523	0.98773

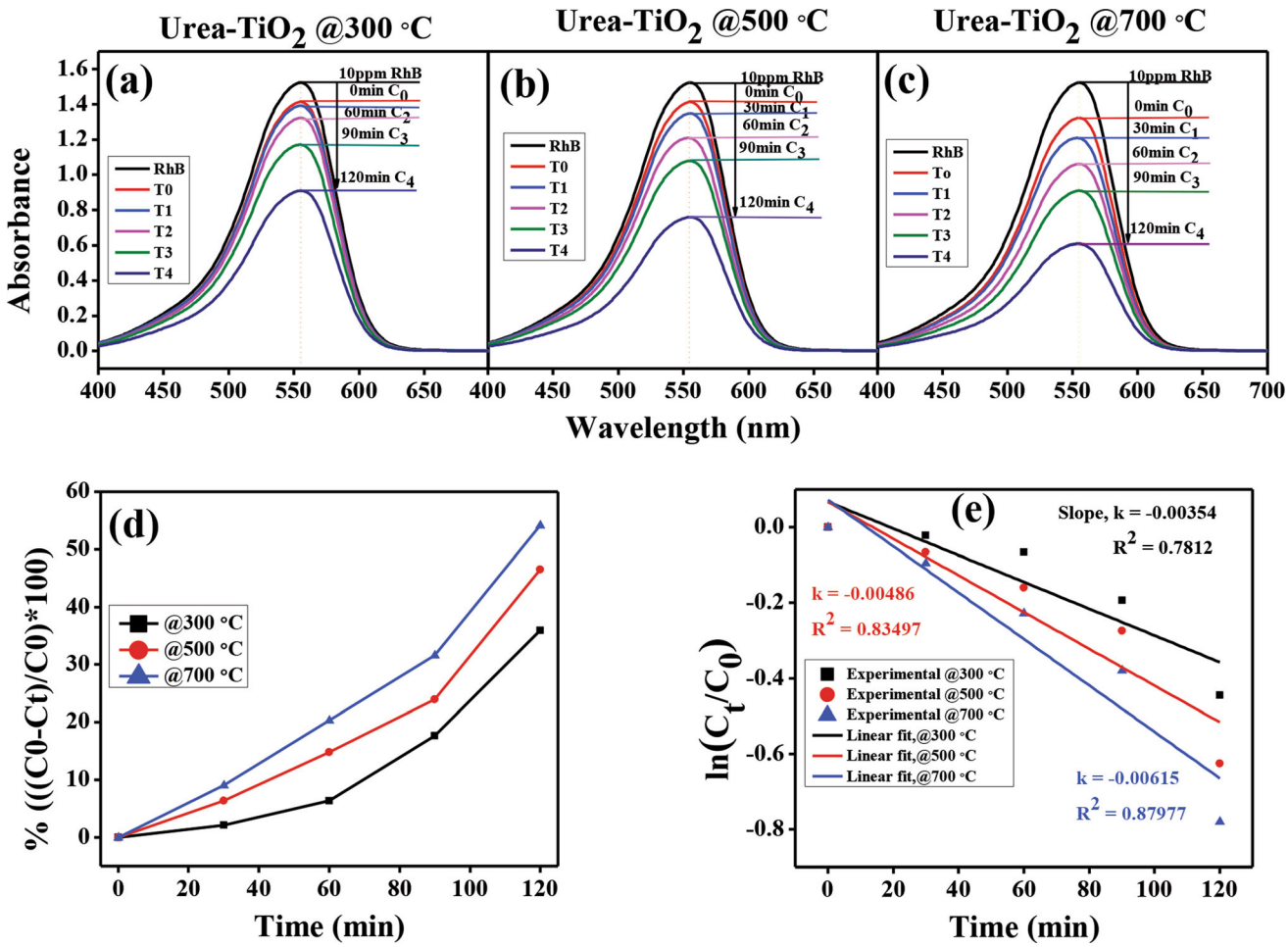

Fig. 8 Photocatalytic degradation of RhB under UV irradiation by samples of urea-TiO_2. Depletion of RhB under UV light for (a) 300 °C, (b) 500 °C, and (c) 700 °C, (d) percentage degradation against time for samples annealed at 300, 500, and 700 °C, (e) $\ln(C_t/C_0)$ against the time of degradation and determination of rate constant Adjusted R^2 (model accuracy) for the different calcined samples

carrier recombination and inhibits photocatalytic activity (Ref 62). Though the rate of photocatalytic degradation was enhanced with an increase in calcination temperature, according to the results displayed in Table 3, the highest rate was obtained at 500 °C from this study. The results also tally with those obtained by other authors (Ref 63, 64).

3.4.2 Rhodamine-B (RhB) degradation. Further tests were conducted to confirm the photocatalytic and self-cleaning functionality of the various calcined urea-TiO_2 samples by letting the pieces degrade 10 ppm of RhB dye in an aqueous solution. RhB, with the chemical formula ($C_{28}H_{31}ClN_2O_3$), is one essential component of the xanthene dyes, which is reportedly a stronger organic pollutant than MB (Ref 65, 66). Fifty milligrams of each sample was equally dissolved in 100 ml of 10 ppm aqueous solution of RhB and kept stirring under UV light throughout the experiment. Initially, the samples were agitated in the dark for 30 minutes for proper adsorption and desorption before the UV lamp was switched on. Ten milliliters of samples was taken out every 30 minutes and was analyzed for RhB concentration reduction using a Shimadzu UV-1900 UV–Vis spectrophotometer. Plots of reduction in RhB concentration, percentage degradation against time, and $\ln(C_t/C_0)$ against the time for the different calcined samples are shown in Figure 8. All the pieces degraded the RhB dye. Equation 7 was used to determine each sample's first-order rate constant, as shown in Figure 8(e). It is observed that the

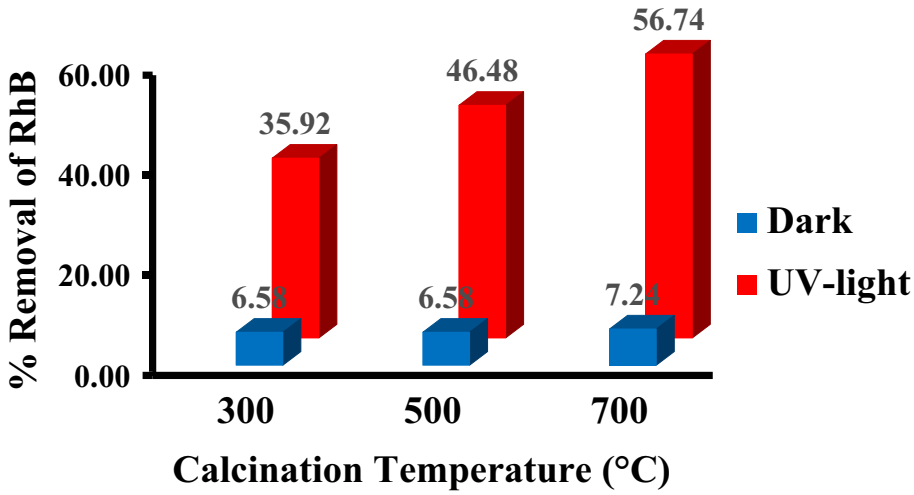

Fig. 9 Percentage of RhB removed by the various samples during the dark and under UV irradiation

model calcined at 700 °C still had the fastest degradation rate (k = 0.00615) than to those at 300 and 500 °C (k = 0.00354 and k = 0.00486), respectively.

The total concentrations of the RhB dye removed by the various samples are shown in Figure 9 for both the first 30 minutes in the dark and the 120 minutes under UV irradiation. The pieces calcined at 700 °C removed above 56% of the RhB dye, which was the highest compared to 35.92 and 46.48 % for urea-TiO_2 calcined at 300 and 500 °C, respectively. After calcination at higher temperatures, the phase structural transformation from anatase to rutile exhibited better photocatalytic performance for RhB since electrons were transferred from anatase to rutile, providing wide electron–hole separation and suppressing the charge carrier recombination (Ref 67). Additionally, when TiO_2 is doped with urea, the presence of nitrogen extends its absorption capability into the visible spectrum, improving photocatalytic performance and enhancing self-cleaning functionality (Ref 68). The urea-TiO_2 material has potential applications in catalysis, sensing devices, self-cleaning, and solar cells.

The photodegradation or self-cleaning findings are for MB and RhB concentrations of 10 ppm and 5 weight percent urea dopant in TiO_2 catalyst. The self-cleaning test proved that calcination temperature has an impact on the functionality of urea-doped TiO_2 in photocatalytic applications. The material degraded both MB and RhB dyes, though the observation is that a longer time is needed to lessen RhB than MB completely. Bakre et al. observed a similar effect in their study (Ref 34). Up to 83% of MB dye was degraded within 120 minutes of reaction time, while only 56.74 % of RhB was degraded within the same interval.

4. Conclusion

An in situ heat-assisted sol–gel method was used to synthesize urea-TiO_2 nanoparticles, and the effect of calcination temperature on its self-cleaning functionality was examined. The structural analysis demonstrates unequivocally how calcination temperature and nitrogen presence modify TiO_2's crystal structure and crystalline size, thereby influencing its self-cleaning ability. The optical analysis revealed that the optical bandgap reduced from 3.29 eV at 300 °C to 3.09 eV at 700 °C. The photoluminescence peaks for the sample calcined at 500 °C reflected high crystallinity of the anatase phase, which also agreed with the results of the XRD peaks. This resulted from the fact that most organic remnants have been eliminated, while the N-dopant is still kept and that the anatase phase is better crystalline at 500 °C than at 300 °C. The absorption ability was extended into the visible-light region, facilitated by the presence of nitrogen in the Urea dopant. The sample calcined at 700 °C had the highest photodegradation rate constant from the self-cleaning test. This was possibly so because of the drop in bandgap and the fact that at a higher calcination temperature of 700 °C, most organic residues are removed from the specimen surface, improving absorption and boasting photocatalytic or self-cleaning functionality. Also, the phase structure transformation from anatase to rutile after calcination at higher temperatures allowed for wide electron–hole separation and inhibited charge carrier recombination. This decrease in recombination results in a rise in photocatalytic activity due to increased charge carrier lifetime. Therefore, improved calcination temperature positively affected the self-cleaning ability of the synthesized urea-TiO_2. The urea-TiO_2 material has potential applications in catalysis, solar panel surfaces, sensing devices, self-cleaning tiles, concrete, car paints self-cleaning, and solar cells.

Acknowledgment

The authors appreciate the financial support of the National Research Foundation South Africa, the Global Excellence and Stature Awards, and the University Research Council of the University of Johannesburg, South Africa.

Author Contribution

All authors contributed to the study's conception and design. Mr. Valantine Takwa Lukong performed the conceptualization, formal analysis, and first draft. Mr. Christopher Nonso Chukwuati developed a methodology, data acquisition, and investigation. Preliminary supervision, review, and editing were performed by Dr. Ukoba Kingsley, and Prof. Tien-Chien Jen carried out final

editing, source of funding, and project administration. All authors read and approved the final manuscript.

Funding

Open access funding provided by University of Johannesburg.

Data Availability

Data will be available upon request.

Conflict of interest

The authors, at this moment, declare that there exist no conflicting financial interests that could affect this work.

Open Access

References

1. M. Sakhuja, J. Son, H. Yang, C.S. Bhatia, and A.J. Danner, Outdoor Performance and Durability Testing of Antireflecting and Self-Cleaning Glass for Photovoltaic Applications, *Sol. Energy*, 2014, **110**, p 231–238. https://doi.org/10.1016/j.solener.2014.07.003
2. P.F. Rios, H. Dodiuk, and S. Kenig, Self-Cleaning Coatings, *Surf Eng*, 2009, **25**(2), p 89–92. https://doi.org/10.1179/174329409X373710
3. N. Mufti, I. K. Laila, A. Fuad, in *The Effect of TiO_2 Thin Film Thickness on Self-Cleaning Glass Properties*. Journal of Physics: Conference Series (Vol. 853, No. 1, p. 012035). (IOP Publishing, 2017) https://doi.org/10.1088/1742-6596/853/1/012035
4. A.M. Zaky, and B.P. Chaplin, Porous Substoichiometric TiO_2 Anodes as Reactive Electrochemical Membranes for Water Treatment, *Environ. Sci. Technol.*, 2013, **47**(12), p 6554–6563. https://doi.org/10.1021/es401287e
5. E.I. Cedillo-González, J.M. Hernández-López, J.J. Ruiz-Valdés, V. Barbieri, and C. Siligardi, Self-Cleaning TiO_2 Coatings for Building Materials: The Influence of Morphology and Humidity in the Stain Removal Performance, *Construct Build Mater*, 2020, **237**, p 117692. https://doi.org/10.1016/j.conbuildmat.2019.117692
6. M.M. Nerandzic, J.L. Cadnum, M.J. Pultz, and C.J. Donskey, Evaluation of an Automated Ultraviolet Radiation device for Decontamination of Clostridium Difficile and Other Healthcare-Associated Pathogens in Hospital Rooms, *BMC Infect. Dis.*, 2010, **10**(1), p 1–8. https://doi.org/10.1186/1471-2334-10-197
7. D.M. Mircea, in *Self-Cleaning Concrete for Landscaping Applications*. MATEC Web of Conferences (Vol. 289, p. 05004). (EDP Sciences, 2019) https://doi.org/10.1051/matecconf/201928905004
8. S. Guldin, P. Kohn, M. Stefik, J. Song, G. Divitini, F. Ecarla, C. Ducati, U. Wiesner, and U. Steiner, Self-Cleaning Antireflective Optical Coatings, *Nano lett*, 2013, **13**(11), p 5329–5335. https://doi.org/10.1021/nl402832u
9. S.H. Astaneh, G. Jursich, C. Sukotjo, and C.G. Takoudis, Surface and Subsurface Film Growth of Titanium Dioxide on Polydimethylsiloxane by Atomic Layer Deposition, *Appl. Surf. Sci.*, 2019, **493**, p 779–786. https://doi.org/10.1016/j.apsusc.2019.07.029
10. M.A. Malik, M.Y. Wani, and M.A. Hashim, Micro Emulsion Method: A novel Route to Synthesize Organic and Inorganic Nanomaterials: First Nano Update, *Arab. J. Chem.*, 2012, **5**(4), p 397–417. https://doi.org/10.1016/j.arabjc.2010.09.027
11. B.K. Mutuma, G.N. Shao, W.D. Kim, and H.T. Kim, Sol–gel synthesis of Mesoporous anatase–brookite and anatase–brookite–rutile TiO_2 nanoparticles and their Photocatalytic Properties, *J Coll Interface Sci*, 2015, **442**, p 1–7. https://doi.org/10.1016/j.jcis.2014.11.060
12. V. Abbasi-Chianeh, A. Mohammadzadeh, and N.N. Ilkhechi, Modeling the Response of Optical and Hydrophobic Properties of Codoped TiO_2 Thin Films, *J. Aust. Ceram. Soc.*, 2019, **55**, p 355–362. https://doi.org/10.1007/s41779-018-0241-0
13. V.T. Lukong, K. Ukoba, and T.C. Jen, Review of Self-Cleaning TiO_2 Thin Films Deposited with Spin Coating, *Int J Adv Manuf Technol*, 2022, **122**(9–10), p 3525–3546. https://doi.org/10.1007/s00170-022-10043-3
14. N.N. Ilkhechi, N. Ghobadi, B.K. Kaleji, and M. Mozammel, Effect of Sn and La Doping on Optical and Hydrophilic Properties of TiO_2 thin film, *Opt. Quant. Electron.*, 2016, **48**, p 1–12. https://doi.org/10.1007/s11082-016-0677-9
15. N.N. Ilkhechi, Z. Azar, M. Khajeh, and M. Mozammel, Enhanced Structural, Optical and Super-Hydrophilic Properties of TiO_2 Thin Film Co-Doped by V and Sn, *J. Mater. Sci.: Mater. Electron.*, 2016, **27**, p 10541–10549. https://doi.org/10.1007/s10854-016-5147-4
16. M. Mozammel, N.N. Ilkhechi, E.F. Tanouraghaj, and E. Rezaei, Evaluation of the Effect of high Concentration of Dopant (Cr, Sn) on Structural, Optical, and Wettability Properties of ZnO Thin Films, *J. Aust. Ceram. Soc.*, 2019, **55**, p 999–1007. https://doi.org/10.1007/s41779-019-00312-y
17. M. Shaban, and A.M. El Sayed, Effects of Lanthanum and Sodium on the Structural, Optical and Hydrophilic Properties of sol–gel derived ZnO films: A comparative study, *Mater. Sci. Semicond. Process.*, 2016, **41**, p 323–334. https://doi.org/10.1016/j.mssp.2015.09.002
18. N.N. Ilkhechi, N. Ghobadi, and F. Yahyavi, Enhanced Optical and Hydrophilic Properties of V and La Co-Doped ZnO Thin Films, *Opt. Quant. Electron.*, 2017, **49**, p 1–10. https://doi.org/10.1007/s11082-016-0867-5
19. N.N. Ilkhechi, A. Ahmadi, and B.K. Kaleji, Optical and Structural Properties of Nanocrystalline Anatase Powders Doped by Zr, Si and Cu at High Temperature, *Opt. Quant. Electron.*, 2015, **47**, p 2423–2434. https://doi.org/10.1007/s11082-015-0120-7
20. Y. Zhu, R. Wang, W. Zhang, H. Ge, and L. Li, CdS and PbS Nanoparticles Co-Sensitized TiO_2 Nanotube Arrays and Their Enhanced Photoelectrochemical Property, *Appl. Surf. Sci.*, 2014, **315**, p 149–153. https://doi.org/10.1016/j.apsusc.2014.07.116
21. A. Hajjaji, S. Jemai, A. Rebhi, K. Trabelsi, M. Gaidi, A.N. Alhazaa, M.A. Al-Gawati, M.A. El Khakani, and B. Bessais, Enhancement of Photocatalytic and Photoelectrochemical Properties of TiO_2 Nanotubes Sensitized by SILAR-Deposited PbS Nanoparticles, *J Mater*, 2020, **6**(1), p 62–69. https://doi.org/10.1016/j.jmat.2019.12.002
22. N.N. Ilkhechi, N. Ghobadi, and M.R. Akbarpour, Enhanced Optical and Photo Catalytic Properties of V and La co doped TiO_2 Nanoparticles, *J. Mater. Sci.: Mater. Electron.*, 2017, **28**, p 6426–6434. https://doi.org/10.1007/s10854-016-6328-x
23. X. Zhang, F. Wang, H. Huang, H. Li, X. Han, Y. Liu, and Z. Kang, Carbon Quantum Dot Sensitized TiO_2 Nanotube Arrays for Photoelectrochemical Hydrogen Generation Under Visible Light, *Nanoscale*, 2013, **5**(6), p 2274–2278. https://doi.org/10.1039/C3NR34142A
24. Y.C. Hong, C.U. Bang, D.H. Shin, and H.S. Uhm, Band Gap Narrowing of TiO_2 by Nitrogen Doping in Atmospheric Microwave Plasma, *Chem. Phys. Lett.*, 2005, **413**(4–6), p 454–457. https://doi.org/10.1016/j.cplett.2005.08.027
25. S. Hoang, S. Guo, N.T. Hahn, A.J. Bard, and C.B. Mullins, Visible Light Driven Photoelectrochemical Water Oxidation on Nitrogen-Modified TiO_2 Nanowires, *Nano Lett.*, 2012, **12**(1), p 26–32. https://doi.org/10.1021/nl2028188
26. A. Ranjitha, N. Muthukumarasamy, M. Thambidurai, R. Balasundaraprabhu, and S. Agilan, Effect of Annealing Temperature on Nanocrystalline TiO_2 thin Films Prepared by Sol–Gel Dip Coating Method, *Optik*, 2013, **124**(23), p 6201–6204. https://doi.org/10.1016/j.ijleo.2013.04.085

27. N. Najibi-Ilkhechi, B. Koozegar-Kaleji, and E. Salahi, Effect of Heating Rate on Structural and Optical Properties of Si and Mg co-doped ZrO_2 Nanopowders, *Opt. Quant. Electron.*, 2015, **47**, p 1187–1195. https://doi.org/10.1007/s11082-014-9975-2
28. M.G. Kim, J.M. Kang, J.E. Lee, K.S. Kim, K.H. Kim, M. Cho, and S.G. Lee, Effects of Calcination Temperature on the Phase Composition, Photocatalytic Degradation, and Virucidal Activities of TiO_2 Nanoparticles, *ACS Omega*, 2021, **6**(16), p 10668–10678. https://doi.org/10.1021/acsomega.1c00043
29. N.N. Ilkhechi, and B.K. Kaleji, High Temperature Stability and Photocatalytic Activity of Nanocrystalline Anatase Powders with Zr and Si co-Dopants, *J. Sol-Gel. Sci. Technol.*, 2014, **69**, p 351–356. https://doi.org/10.1007/s10971-013-3224-1
30. N.H. Aprilita, D. Amalia, and E.T. Wahyuni, Removal of the Hazardous Congo Red Dye Through Degradation Under Visible Light Photo Catalyzed by C, N Co-doped TiO_2 Prepared From Chicken Egg White, *Sci World J*, 2022 https://doi.org/10.1155/2022/2613841
31. N.N. Ilkhechi, B.K. Kaleji, E. Salahi, and N. Hosseinabadi, Comparison of Optical and Structural Properties of Cu Doped and Cu/Zr co-doped TiO_2 Nanopowders Calcined at Various Temperatures, *J. Sol-Gel. Sci. Technol.*, 2015, **74**, p 765–773. https://doi.org/10.1007/s10971-015-3661-0
32. N.N. Ilkhechi, A.R. Aghjehkohal, E.F. TanourAghaj, and M. Mozammel, Enhanced Optical and Hydrophilic Properties of Si and Cd co-Doped TiO_2 Thin Films, *J. Mater. Sci.: Mater. Electron.*, 2017, **28**, p 4598–4605. https://doi.org/10.1007/s10854-016-6097-6
33. L. Zhu, J. Xie, X. Cui, J. Shen, X. Yang, and Z. Zhang, Photoelectrochemical and Optical Properties of N-Doped TiO_2 Thin Films Prepared By Oxidation of Sputtered TiNx Films, *Vacuum*, 2010, **84**(6), p 797–802. https://doi.org/10.1016/j.vacuum.2009.10.040
34. P.V. Bakre, S.G. Tilve, and R.N. Shirsat, Influence of N Sources on the Photocatalytic Activity of N-Doped TiO_2, *Arab. J. Chem.*, 2020, **13**(11), p 7637–7651. https://doi.org/10.1016/j.arabjc.2020.09.001
35. T. Xu, M. Wang, and T. Wang, Effects of N Doping on the Microstructures and Optical Properties of TiO2., *J Wuhan Univ Technol Mater Sci.*, 2019, **34**, p 55–63
36. X. Yang, Q. Jia, J. Pang, Y. Yang, S. Zheng, J. Jia, and Z. Qin, Hierarchical Porous N-TiO_2/Carbon Foam Composite for Enhancement of Photodegradation Activity Under Simulated Sunlight, *Diamond Related Mater*, 2022, **128**, p 109234. https://doi.org/10.1016/j.diamond.2022.109234
37. Y. Ruzmanova, M. Stoller, M. Bravi, and A. Chianese, A Novel Approach for the Production of Nitrogen Doped TiO_2 Nanoparticles, *Chem Eng Trans*, 2015, **43**, p 721–726. https://doi.org/10.3303/CET1543121
38. J.G. Mahy, V. Cerfontaine, D. Poelman, F. Devred, E.M. Gaigneaux, B. Heinrichs and S.D. Lambert, Highly Efficient Low-Temperature N-Doped TiO_2 Catalysts for Visible Light Photocatalytic Applications, *Materials*, 2018, **11**(4), p 584. https://doi.org/10.3390/ma11040584
39. T. Goto, J. Shin, T. Yokoi, S.H. Cho, and T. Sekino, Photocatalytic Properties and Controlled Morphologies of TiO_2-Modified Hydroxyapatite Synthesized by the Urea-Assisted Hydrothermal Method, *Powder Technol.*, 2020, **373**, p 468–475. https://doi.org/10.1016/j.powtec.2020.06.062
40. J. Marques, T.D. Gomes, M.A. Forte, R.F. Silva, and C.J. Tavares, A New Route for the Synthesis of Highly-Active N-doped TiO_2 Nanoparticles for Visible Light Photocatalysis Using Urea as Nitrogen Precursor, *Catal. Today*, 2019, **326**, p 36–45. https://doi.org/10.1016/j.cattod.2018.09.002
41. J. Ananpattarachai, P. Kajitvichyanukul, and S. Seraphin, Visible Light Absorption Ability and Photocatalytic Oxidation Activity of Various Interstitial N-Doped Tio_2 Prepared From Different Nitrogen Dopants, *J. Hazard. Mater.*, 2009, **168**(1), p 253–261. https://doi.org/10.1016/j.jhazmat.2009.02.036
42. B. Choudhury, and A. Choudhury, Local Structure Modification and Phase Transformation of TiO_2 Nanoparticles Initiated by Oxygen Defects, Grain Size, and Annealing Temperature, *Int Nano Lett*, 2013, **3**(1), p 1–9. https://doi.org/10.1186/2228-5326-3-55
43. C.A. Beaudette, Q. Tu, M. Ali Eslamisaray, and U.R. Kortshagen, Plasma-Synthesized Nitrogen-doped Titanium Dioxide Nanoparticles with Tunable Visible Light Absorption and Photocatalytic Activity, *ASME Open J Eng*, 2022, **10**(1115/1), p 4053338
44. R. Chauhan, A. Kumar, and R.P. Chaudhary, Structural and Optical Characterization of Zn doped TiO_2 Nanoparticles Prepared by Sol–gel Method, *J. Sol-Gel. Sci. Technol.*, 2012, **61**(3), p 585–591. https://doi.org/10.1007/s10971-011-2664-8
45. V.T. Lukong, K.O. Ukoba, and T.C. Jen, Heat-Assisted Sol–gel Synthesis of TiO_2 Nanoparticles Structural, Morphological and Optical Analysis for Self-Cleaning Application, *J King Saud Univ-Sci*, 2022, **34**(1), p 101746. https://doi.org/10.1016/j.jksus.2021.101746
46. M. Lal, P. Sharma, and C. Ram, Calcination Temperature Effect on Titanium Oxide (TiO_2) Nanoparticles Synthesis, *Optik*, 2021, **241**, p 166934. https://doi.org/10.1016/j.ijleo.2021.166934
47. V.T. Lukong, K. Ukoba, K.O. Yoro, and T.C. Jen, Annealing Temperature Variation and its Influence on the Self-Cleaning Properties of TiO_2 Thin Films, *Heliyon*, 2022, **8**(5), p e09460. https://doi.org/10.1016/j.heliyon.2022.e09460
48. L.K. Preethi, R.P. Antony, T. Mathews, L. Walczak, and C.S. Gopinath, A Study on Doped Heterojunctions in TiO_2 Nanotubes: an Efficient Photocatalyst for Solar Water Splitting, *Sci. Rep.*, 2017, **7**(1), p 1–15. https://doi.org/10.1038/s41598-017-14463-0
49. Q. Chen, A. Ozkan, B. Chattopadhyay, K. Baert, C. Poleunis, A. Tromont, R. Snyders, A. Delcorte, H. Terryn, M.P. Delplancke-Ogletree, and Y.H. Geerts, N-Doped TiO_2 Photocatalyst Coatings Synthesized by a Cold Atmospheric Plasma, *Langmuir*, 2019, **35**(22), p 7161–7168. https://doi.org/10.1021/acs.langmuir.9b00784
50. A.A. Melvin, K. Illath, T. Das, T. Raja, S. Bhattacharyya, and C.S. Gopinath, M-Au/TiO_2 (M= Ag, Pd, and Pt) Nanophotocatalyst for Overall Solar Water Splitting: Role of Interfaces, *Nanoscale*, 2015, **7**(32), p 13477–13488. https://doi.org/10.1039/c5nr03735b
51. A. León, P. Reuquen, C. Garín, R. Segura, P. Vargas, P. Zapata, and P.A. Orihuela, FTIR and Raman Characterization of TiO_2 Nanoparticles Coated with Polyethylene Glycol as Carrier for 2-Methoxyestradiol, *Appl. Sci.*, 2017, **7**(1), p 49. https://doi.org/10.3390/app7010049
52. C. Niu, X. Dong, and M. Qi, Enhanced Electrorheological Properties of Elastomers Containing TiO_2/Urea Core–Shell Particles, *ACS Appl. Mater. Interfaces.*, 2015, **7**(44), p 24855–24863. https://doi.org/10.1021/acsami.5b08127
53. R.P. Barkul, V.B. Koli, V.B. Shewale, M.K. Patil and S.D. Delekar, Visible Active Nanocrystalline N-Doped Anatase TiO_2 Particles for Photocatalytic Mineralization Studies, *Mater. Chem. Phys.*, 2016, **173**, p 42–51. https://doi.org/10.1016/j.matchemphys.2016.01.035
54. J.H. Xu, W.L. Dai, J. Li, Y. Cao, H. Li, H. He, and K. Fan, Simple Fabrication of Thermally Stable Apertured N-Doped TiO_2 Microtubes as a Highly Efficient Photocatalyst Under Visible Light Irradiation, *Catal. Commun.*, 2008, **9**(1), p 146–152. https://doi.org/10.1016/j.catcom.2007.05.043
55. Q. Li, J. Sun, L. Zhuang, X. Xu, Y. Sun, and G. Wang, Effect of Urea Addition on Chitosan Dissolution with [Emim] Ac-Urea Solution System, *Carbohyd. Polym.*, 2018, **195**, p 288–297. https://doi.org/10.1016/j.carbpol.2018.04.097
56. K.H. Chung, B.J. Kim, Y.K. Park, S.C. Kim, and S.C. Jung, Photocatalytic Properties Of Amorphous N-doped TiO_2 Photocatalyst Under Visible Light Irradiation, *Catalysts*, 2021, **11**(8), p 1010. https://doi.org/10.3390/catal11081010
57. X. Pan, X. Gao, X. Chen, H.N. Lee, Y. Liu, R.L. Withers, and Z. Yi, Design Synthesis of Nitrogen-Doped TiO2@ Carbon NANO SHEETS TOWARD SELECTIVE Nitroaromatics Reduction Under Mild Conditions, *ACS Catal.*, 2017, **7**(10), p 6991–6998. https://doi.org/10.1021/acscatal.7b02322.s001
58. D. Komaraiah, P. Madhukar, Y. Vijayakumar, M.R. Reddy, and R. Sayanna, Photocatalytic Degradation Study of Methylene Blue By Brookite TiO_2 Thin Film Under Visible Light Irradiation, *Mater Today: Proc*, 2016, **3**(10), p 3770–3778. https://doi.org/10.1016/j.matpr.2016.11.026
59. R.P. Antony, T. Mathews, J.A. Johnson, D.N. Krishna, S. Dash, and A.K. Tyagi, Kinetics of Dye Destruction Using Electrochemically Synthesized Sunlight Active N-Doped and C and N co-Doped TiO_2 Nanotubular Photocatalysts, *Energy Environ Focus*, 2013, **2**(2), p 139–148. https://doi.org/10.1166/eef.2013.1041
60. H. Li, Y. Hao, H. Lu, L. Liang, Y. Wang, J. Qiu, X. Shi, Y. Wang, and J. Yao, A Systematic Study on Visible-Light N-Doped Tio_2 Photocatalyst Obtained From Ethylenediamine by Sol–Gel Method, *Appl. Surf. Sci.*, 2015, **344**, p 112–118. https://doi.org/10.1016/j.apsusc.2015.03.071
61. F.M. Pesci, G. Wang, D.R. Klug, Y. Li, and A.J. Cowan, Efficient Suppression of Electron–Hole Recombination in Oxygen-Deficient Hydrogen-Treated TiO_2 Nanowires for Photoelectrochemical Water

Splitting, *J Phys Chem C*, 2013, **117**(48), p 25837–25844. https://doi.org/10.1021/jp4099914

62. T.S. Natarajan, V. Mozhiarasi, and R.J. Tayade, Nitrogen Doped Titanium Dioxide (N-Tio_2): Synopsis of Synthesis Methodologies, Doping Mechanisms, Property Evaluation and Visible Light Photocatalytic Applications, *Photochem*, 2021, **1**(3), p 371–410. https://doi.org/10.3390/photochem1030024
63. C.N. Chukwuati, and R.M. Moutloali, Antibacterial Studies of Ag@ HPEI@ GO Nanocomposites and Their Effects on Fouling and Dye Rejection in PES UF Membranes, *Heliyon*, 2022, **8**(11), p e11825. https://doi.org/10.1016/j.heliyon.2022.e11825
64. H. Zhang, K. Cai, H. Liu, and L. Sun, in *Effect of Nitrogen-Doping on Photocatalytic Activity of Nanosized TiO_2 Catalyst*. 2017 5th International Conference on Machinery, Materials and Computing Technology (ICMMCT 2017) (pp. 231-236, 2017). Atlantis Press. https://doi.org/10.2991/icmmct-17.2017.45
65. N. Van Hung, B.T.M. Nguyet, N.H. Nghi, V.T. Nguyen, T.V. Binh, N.T.T. Tu, N.N. Dung, and D.Q. Khieu, Visible Light Photocatalytic Degradation of Organic Dyes Using W-Modified TiO_2/SiO_2 Catalyst, *Vietnam J Chem*, 2021, **59**(5), p 620–638. https://doi.org/10.1002/vjch.202100016
66. W. Peng, C. Yang, and J. Yu, Bi_2O_3 and gC_3N_4 Quantum Dot Modified Anatase Tio_2 Heterojunction System for Degradation of Dyes Under Sunlight Irradiation, *RSC Adv.*, 2020, **10**(2), p 1181–1190
67. Y. Bao, R. Guo, M. Gao, Q. Kang, and J. Ma, Morphology Control of 3d Hierarchical Urchin-Like Hollow Sio_2@ Tio_2 Spheres For Photocatalytic Degradation: Influence of Calcination Temperature, *J Alloys Compd*, 2021, **853**, p 157202. https://doi.org/10.1016/j.jallcom.2020.157202
68. M. Nasirian, and M. Mehrvar, Photocatalytic Degradation of Aqueous Methyl Orange Using Nitrogen-Doped Tio_2 Photocatalyst Prepared by Novel Method of Ultraviolet-Assisted Thermal Synthesis, *J. Environ. Sci.*, 2018, **66**, p 81–93. https://doi.org/10.1016/j.jes.2017.05.032